British Journal of Cancer www.nature.com/bjc

ARTICLE

Heat-shock protein 90α protects NME1 against degradation and suppresses metastasis of breast cancer

Yanchao Zhang[1,2,8], Guomeng Zhao[3,8], Liting Yu[4], Xindong Wang[5], Yao Meng[5], Jinlei Mao[5], Ziyi Fu[6], Yongmei Yin[6]✉, Jinyao Li[1]✉, Xun Wang[7]✉ and Changying Guo[1]✉

BACKGROUND: NME1 has been exploited as a potential translational target for decades. Substantial efforts have been made to upregulate the expression of NME1 and restore its anti-metastasis function in metastatic cancer.
METHODS: Cycloheximide (CHX) chase assay was used to measure the steady-state protein stability of NME1 and HSP90α. The NME1-associating proteins were identified by immunoprecipitation combined with mass spectrometric analysis. Gene knockdown and overexpression were employed to examine the impact of HSP90AA1 on intracellular NME1 degradation. The motility and invasiveness of breast cancer cells were examined in vitro using wound healing and transwell invasion assays. The orthotopic spontaneous metastasis and intra-venous experimental metastasis assays were used to test the formation of metastasis in vivo, respectively.
RESULTS: HSP90α interacts with NME1 and increases NME1 lifetime by impeding its ubiquitin-proteasome-mediated degradation. HSP90α overexpression significantly inhibits the metastatic potential of breast cancer cells in vitro and in vivo. A novel cell-permeable peptide, OPT22 successfully mimics the HSP90α function and prolongs the life span of endogenous NME1, resulting in reduced metastasis of breast cancer.
CONCLUSION: These results not only reveal a new mechanism of NME1 degradation but also pave the way for the development of new and effective approaches to metastatic cancer therapy.

British Journal of Cancer (2023) 129:1679–1691; https://doi.org/10.1038/s41416-023-02435-3

INTRODUCTION

Cancer metastasis is the leading cause of cancer morbidity and mortality. It is important to elucidate the cellular and molecular events that drive cancer metastasis and develop effective strategies or drugs for the treatment of metastatic cancer. Metastasis suppressor genes (MSGs) have been identified by their ability to inhibit overt metastasis in a secondary organ without affecting the growth of the primary tumour [1]. NME1 is the first MSG discovered in 1988 by differential colony hybridisation [2]. A significant negative correlation between the expression level of NME1 and metastatic potential has been observed in a variety of cancers, including breast, liver, colon and melanoma cancers [3]. NME1 plays a prominent role in the regulation of the metastatic cascade: cell migration, invasion, proliferation and apoptosis [4–6]. With its crucial role in the regulation of metastasis, NME1 has been considered to be a promising prognostic marker and therapeutic target in the diagnosis and treatment of metastatic cancer [6]. Experimental and clinical data have shown that an augmentation in the intracellular abundance of NME1 results in significant inhibition of metastasis [4, 6]. Most therapeutic strategies aimed at directly boosting the protein level in metastatic cancer cells have focused on manipulating the expression of NME1, by transcriptional transactivation, gene therapy or protein therapy. For example, glucocorticoid receptor (GR) binding sites are identified in the promoter region of the NME1 gene. High doses of a specific ligand of GR, medroxyprogesterone acetate (MPA) upregulate NME1 transcription, and as a consequence, the application of MPA in metastatic cancer therapy is currently in clinical trials [7]. To promote NME1 expression in metastases, an adeno-associated virus (AAV) or specially designed nano-vectors have been developed to deliver this gene to the target tissues [6]. The recombinant NME1 protein fused with macromolecule transduction domains (MTD) improves protein uptake by cells and animal tissues, resulting in a declined incidence of metastasis at least in animal models [8]. Theoretically, inhibition of protein degradation or prolongation of the protein life span is also an effective and feasible strategy with which to maintain a high level of endogenous NME1. However, our limited understanding of the

[1]Xinjiang Key Laboratory of Biological Resources and Genetic Engineering, College of Life Science and Technology, Xinjiang University, Urumqi, People's Republic of China. [2]Wuxi Cancer Institute, Affiliated Hospital of Jiangnan University, Wuxi, People's Republic of China. [3]Institute of Modern Biology, Nanjing University, Nanjing, People's Republic of China. [4]Department of Protein and Antibody Engineering, School of Pharmacy, Binzhou Medical University, Yantai, People's Republic of China. [5]School of Life Science and Technology, China Pharmaceutical University, Nanjing, People's Republic of China. [6]Department of Oncology, The First Affiliated Hospital of Nanjing Medical University, Nanjing People's Hospital, Nanjing, People's Republic of China. [7]Department of Hepatobiliary Surgery, National Cancer Center, National Clinical Research Center for Cancer, Chinese Academy of Medical Sciences and Peking Union Medical College, Beijing, People's Republic of China. [8]These authors contributed equally: Yanchao Zhang, Guomeng Zhao.
✉email: ym.yin@hotmail.com; ljyxju@xju.edu.cn; wangxun301gdwk@163.com; guocy74@gmail.com

Received: 23 November 2022 Revised: 28 August 2023 Accepted: 11 September 2023
Published online: 20 September 2023

degradation pathways of NME1 impedes its application in metastatic cancer therapy. There are published reports that the NME1 protein undergoes different pathways of degradation. Chen et al. for example, demonstrated that the ubiquitin E3 ligase SCF-FBXO24 catalyses ubiquitylation of NME1 at K56 thus facilitating its proteasomal degradation [9]. Fiore et al. found that the oncogene c-Abl and Arg induce cathepsin-mediated lysosomal degradation of the NME1 [10]. Additionally, the hepatitis C Virus (HCV) core protein has been found to promote SUMOylation (attachment of a small ubiquitin-like modifier) of NME1 with SUMO2 and SUMO3 and its degradation [11, 12], although the relationship between SUMOylation and degradation of NME1 remains unclear.

In our study, we demonstrated that heat-shock protein 90α encoded by the HSP90AA1 gene stabilises NME1 protein in breast cancer cells. Overexpression of HSP90AA1 protects endogenous NME1 protein against degradation, resulting in decreased metastasis dissemination in vitro and formation of metastasis in vivo. Furthermore, the specific cell-permeable peptide which mimics the interaction region of HSP90α with NME1 also increases the lifetime of the NME1 protein and inhibits metastasis of breast cancer in the different mouse models. Our study not only assists our understanding of the functional pathway of NME1 degradation but also paves the way to the development of a novel strategy or a drug with which to treat metastatic cancer.

RESULTS

Intracellular abundance of NME1 is strictly regulated by protein degradation

Humans have at least 10 members of the NME family and the two most abundant are NME1 and NME2. Although they share 88% amino acid identity, two isoforms are functionally distinct. Immunoblotting probed with anti-NME1/2 antibody (A0259, Abclonal) which can recognise both isoforms was used to examine the protein abundance of NME1 and NME2 in a series of breast cancer cell lines, including luminal A (MCF7, T47D), human epithelial receptor 2 (HER2) positive (MCF10CA1a, BT474), and triple-negative (MDA-MB-231, MDA-MB-468) subtypes according to the status of oestrogen receptor (ER), progesterone receptor (PR) and HER2 [13]. It is reported that luminal cell lines are less aggressive and metastatic than HER2 and triple-negative cell lines [14, 15]. In addition to a negative correlation of the expression of the two NME isoforms with the known metastatic potential of these cells, consistent with previous report [16], we also found that the expression level of NME1 was lower than that of NME2 in most cell lines (Fig. 1a). This difference may be ascribed to the efficiency of the transcriptional initiation of individual promoter of each isoform. To verify this speculation, we assessed the expression levels of two isoforms in engineered breast cancer MCF7 cell lines which stably express exogenous FLAG-tagged NME1 or NME2, respectively. The expression of both exogenous isoforms was controlled by the same promoter (either U6 or CMV promoter). Intriguingly, quantitative reverse transcription PCR (RT-qPCR) analysis showed that the mRNA level of NME1 was higher than that of NME2, while exogenous NME1 exhibited the opposite result at various protein levels (Fig. 1b), indicating that distinct from NME2, the intracellular expression of NME1 is strictly regulated at the protein level and probably undergoes a unique protein degradation pathway.

To evaluate precisely the contribution of known pathways in the degradation of NME1/2, we measured steady-state protein stability by cycloheximide (CHX) chase assays in various breast cancer cell lines in the presence of inhibitors targeting different degradation pathways, including the autophagy inhibitor 3-methyladenine (3-MA), the autophagy/lysosome inhibitor chloroquine (CQ), the SUMOylation inhibitor ML792 and the proteasome inhibitor MG132. Except for MG132, each inhibitor alone barely affected the intracellular abundance of NME1/2 (Fig. S1A, B). CHX prevents protein synthesis by inhibiting the elongation step in protein translation. Upon treatment with CHX, the NME1/2 protein degraded rapidly. Both 3-MA and CQ did not change NME1/2 degradation behaviours. In contrast, the protein stabilities of both isoforms were promoted by MG132 in all tested cell lines, consistent with the notion that the ubiquitin-proteasome pathway (UPP) is the major pathway of selective protein degradation in eukaryotic cells (Figs. 1c and S1C). Similarly, ML792 also has a prolonged life span of NME1/2.

Next, we attempted to identify the domain(s) responsible for NME1 protein stability. Comparison of the primary structures of NME1 and NME2 exhibited high similarity with a difference of only 18 amino acid residues, mainly in two regions (residues 37–43 and 131–150) (Fig. 1d, upper panel) which may account for lifetime difference between NME1 and NME2. Based on sequence analysis, we generated various truncated forms fused with a FLAG tag (Fig. 1d, schematic in bottom panel) to reveal the association of the region(s) with protein degradation. After transiently expressing these truncates in HEK293T cells, we observed that C-terminal deletion (T5 mutant, $\Delta^{131-152}$,) modestly affected protein stability while both deletions (T1 mutant, Δ^{1-20} or T7 mutant, Δ^{21-55}) at the N-terminus resulted in an obvious reduction of protein abundance. MG132 inhibited the degradation of wild type (WT) and T5, and restored the expression of T1 and T7 only slightly. In contrast, ML792 treatment increased the abundance of WT and T5 but could not rescue the degradation of T1 and T7 (Fig. 1e). We further validated the degradation of various truncates in vitro by incubating recombinant proteins with HEK293T cell lysates. The his-tagged recombinant proteins were expressed and purified from *E. coli* using immobilised Ni^{2+} affinity chromatography (Fig. 1f, left panel). Compared with WT, T1, T5 and T7 recombinant proteins degraded faster after incubation with cell lysates, particularly T1 and T7. Neither 3-MA nor CQ inhibited the degradation of all recombinant proteins. However, MG132 prolonged the lifetimes of all recombinant proteins. Interestingly, ML792 also increased the protein stability of WT and T5, but not T1 and T7 (Fig. 1g). Considering that oligomerization of NME1 into a hexametric structure is required for its NDPK and HPK activity and anti-metastasis function [17], we examined effects of various truncations on NME1 oligomerization. We observed that none of the mutants formed hexamers and only T5 is capable of forming at least dimers (Fig. 1f, right panel) in accordance with the lifetime of mutants, implying that protein folding and oligomerization of NME1 may be associated with its stability. Taken together, our data suggested that the intracellular abundance of NME1 is strictly regulated by protein degradation.

HSP90α is positively correlated with the intracellular stability of NME1

To explore the mechanism of NME1 degradation, we performed proteomic analysis of NME1-interacting proteins. The FLAG-tagged NME1 was stably overexpressed in HEK293T cells (Fig. S2A) and co-immunoprecipitation (co-IP) was conducted using anti-FLAG antibody (Fig. S2B). The IP products were then identified by mass spectrometry and followed by GO enrichment analysis. We found that the bioprocesses in which NME1-associating proteins mainly participate include specifically, the regulation of protein stability (Figs. 2a and S2C). The key proteins involved in the regulation of protein stability are two isoforms (HSP90α and HSP90β) of the heat-shock protein 90. It is known that HSP90 functions as a molecular chaperone that assists in correct protein folding and promotes the stabilisation of various proteins [18]. Immunofluorescence staining showed that NME1 was colocalized with HSP90 (Fig. 2b). Co-IP assay using anti-NME1 or anti-HSP90α antibodies also showed that NME1 and HSP90α are partners in the same complex (Fig. 2c). To further verify the association between NME1 and HSP90α, we expressed and purified the recombinant HA-tagged HSP90α and FLAG-tagged

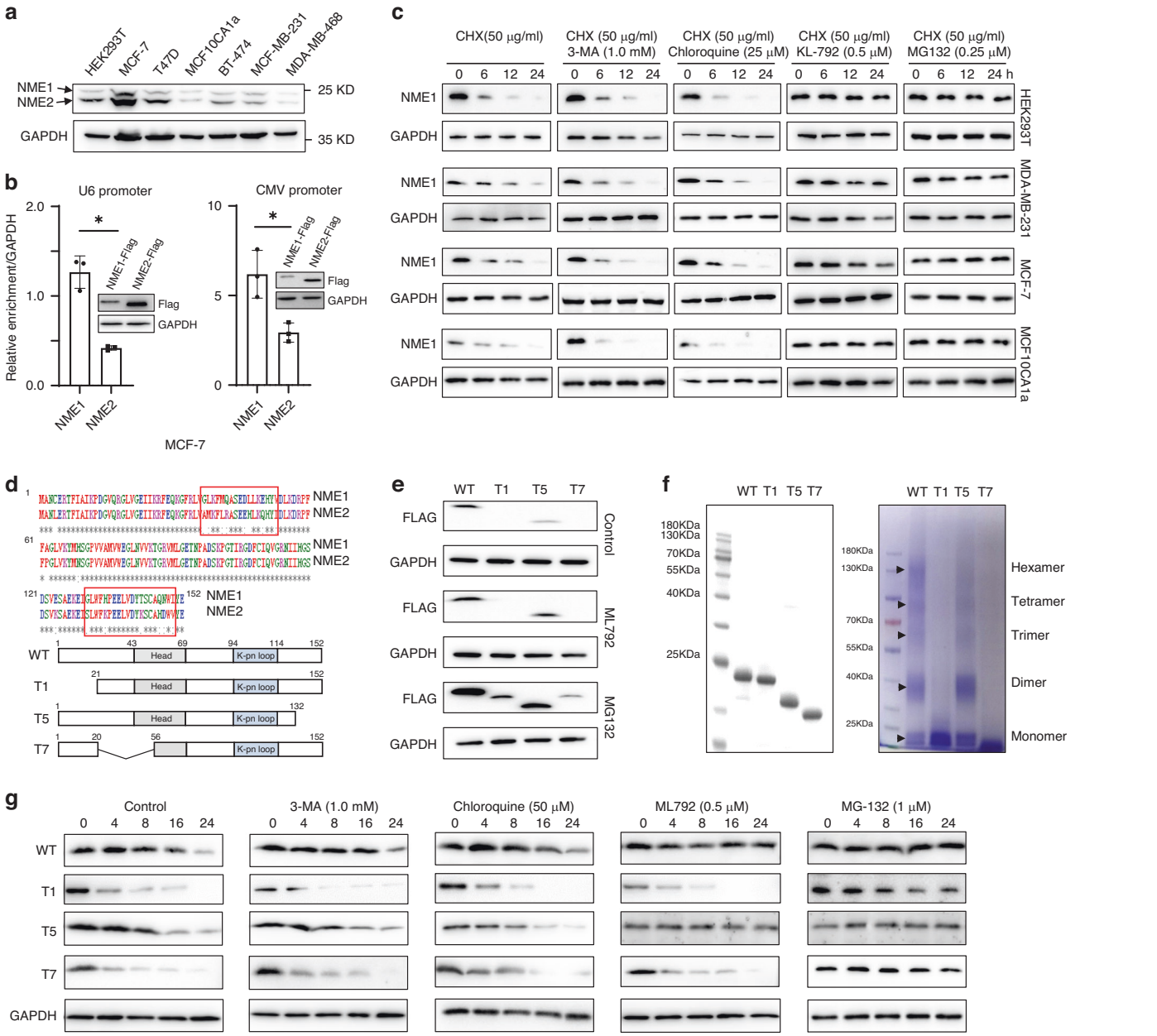

Fig. 1 Protein degradation is an important means to regulate NME1 abundance. a NME1/2 expression level in various types of breast cancer cell lines detected by immunoblotting. **b** Comparison of stable expression of exogenous NME1/2 in MCF-7 cells. NME1 or 2 gene fused with FLAG-tag was stably expressed in MCF-7 cells by lentiviral infection. Their expressions were examined at both mRNA and protein levels. For RT-qPCR, data are mean ± SD of three independent replicates. Student's *t*-test. $*p < 0.05$. **c** Contributions of known degradation pathways to NME1 lifetime in various types of cell lines determined by cycloheximide (CHX) chase assay. NME1 lifetime was examined by immunoblotting upon the treatment of different inhibitors with increasing incubation time. Inhibitors included autophagy inhibitor 3-methyladenine (3-MA), autophagy/lysosome inhibitor chloroquine (CQ), SUMOylation inhibitor ML792 and proteasome inhibitor MG132. **d** The amino acid sequence alignment of NME1 and NME2 (upper panel) and schematic of full length NME1 (WT) and truncated T1, T5 and T7 mutants (bottom panel). **e** The intracellular stability of NME1 WT and mutants exogenously expressed in HEK293T cells. Immunoblotting shows the abundance of NME1 WT and mutants in the presence of ML792 or MG132. **f** SDS-PAGE analysis (left panel) and oligomeric analysis (right panel) of the recombinant WT and truncated proteins of NME1. **g** In vitro measurement of degradation of the recombinant proteins, including NME1 WT, T1, T5 and T7 mutants by immunoblotting. The recombinant proteins were incubated with HEK293T cell lysates for the indicated time. Effects of various inhibitors, such as 3-MA, CQ, ML792 and MG132, on the lifetime of the recombinant proteins were also assessed.

NME1 from *E. coli* followed by in vitro co-IP using anti-HA or anti-FLAG antibody. Reciprocal co-IP results demonstrated a direct interaction between HSP90α and NME1 (Fig. 2d).

To further support the correlation of HSP90α with NME1 expression, we assess the link between HSP90α and NME1 expression as well as the metastatic potential of tumours in breast cancer patients. We collected 6 primary tumour and 6 metastases in the lymph nodes and examined the expression levels of HSP90α and NME1 using immunohistochemistry. As expected, compared to primary tumour tissues, metastases in the lymph nodes expressed lower levels of HSP90α and NME1 (Fig. 2e and S3A). Further, the effect of HSP90 knockdown on NME1

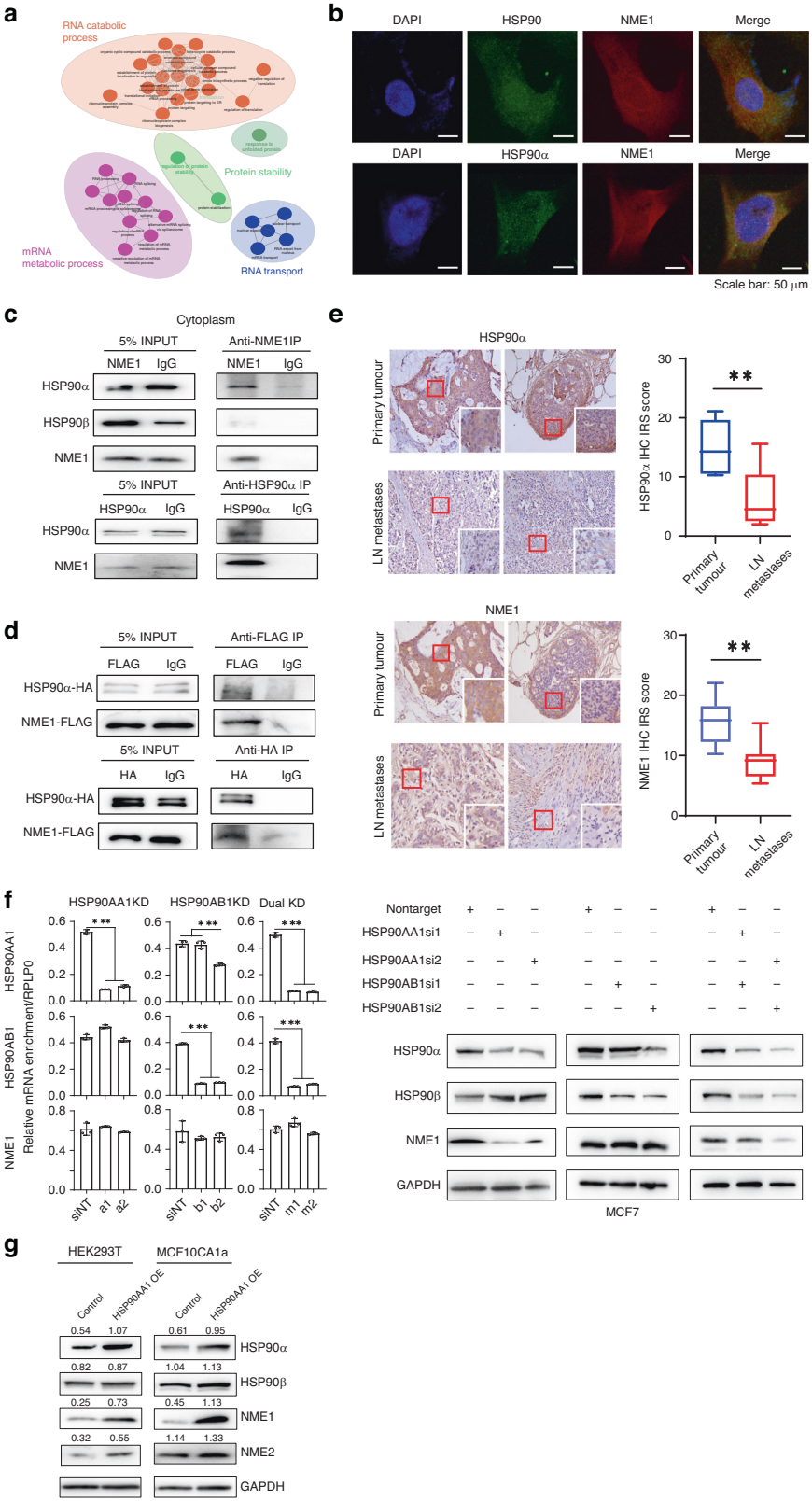

abundance in MCF7 was assessed using siRNA. The qPCR data showed that knockdown of HSP90AA1 encoding HSP90α or HSP90AB1 encoding HSP90β did not affect the mRNA level of NME1 (Fig. 2f, left panel), but HSP90AA1, not HSP90AB1 deficiency attenuated the abundance of intracellular NME1 (Fig. 2f, right panel). At the same time, overexpression of HSP90AA1 in HEK293T and MCF10CA1a cells resulted in an elevated abundance of the NME1 protein (Fig. 2g). Taken together, these results demonstrated that HSP90α directly interacts with NME1 and protects it against degradation.

Fig. 2 HSP90α is positively correlated with the intracellular stability of NME1. a Gene Ontology (GO) enrichment analysis of IP interaction partners with anti-NME1 antibody identified by mass spectrometry. **b** Colocalization of HSP90 with NME1 detected by confocal microscope. Scale bar: 50 μm. **c** Interaction of endogenous NME1 with HSP90α, not HSP90β confirmed by co-IP using HEK293T cell lysates with anti-NME1 antibody and anti-HSP90α antibody, respectively. **d** Direct interaction between NME1 and HSP90α validated by in vitro co-IP using anti-FLAG or anti-HA antibody, respectively. Equal amounts of the recombinant FLAG-tagged NME1 and HA-tagged HSP90α (12 μM) were mixed before immunoprecipitation. **e** IHC representative images of human primary breast cancer tissues and lymph node (LN) metastases using HSP90α antibody (upper panel) or NME1 antibody (bottom panel). Scale bars for ×10 images: 500 μm; scale bars for ×200 images: 20 μm. Statistical analysis of HSP90α IHC IRS score of primary tumour tissues and LN metastases. Student's *t*-test. Data are shown as the mean ± SD. $*p < 0.05$, $**p < 0.01$. **f** Effects of HSP90AA1 or/and HSP90AB1 knockdown (KD) in MCF7 cells on the expression of NME1 at both mRNA (left panel) and protein (right panel) levels. For siRNA mediated HSP90AA1, HSP90AB1 or dual KD, the following sequence-specific siRNAs were used for this study: a1 and a2 against HSP90AA1; b1 and b2 against HSP90AB1, and m1 (mixture of a1 and b1) and m2 (mixture of a2 and b2) against both HSP90AA1 and HSP90AB1; Non-Targeting siRNA (siNT) was used as control. RT-qPCR data are shown as the mean ± SD from three independent replicates. Student's *t*-test. $**p < 0.01$, $***p < 0.001$. **g** Immunoblotting showing effects of HSP90α overexpression on the NME1 expression examined in HEK293T and MCF10CA1a cells. The numbers above the gel lanes represent the relative protein level, which was determined from the band intensity using ImageJ software, and normalised relative to the GAPDH loading control.

SUMOylation-induced NME1 degradation is mediated by HSP90α

Ubiquitination is best known as a signal for proteasome-mediated protein degradation [19]. To confirm that NME1 undergoes proteolysis through UPP, we exogenously expressed FLAG-tagged NME1 in HEK293T cells and determined the ubiquitination status of FLAG-tagged NME1 using co-IP assay with anti-FLAG antibody followed by immunoblotting with anti-ubiquitin antibody. Our data showed a characteristic high molecular weight smear of polyubiquitin molecules conjugated to NME1 and inhibition of the proteasome with MG132 resulted in increased accumulation of ubiquitinated NME1 in 293T cells (Fig. 3a). Next, we investigated the relationship between SUMOylation and ubiquitination of NME1 in the process of NME1 degradation. As a potent and selective inhibitor of the SUMO-activating enzyme (SAE), ML792 promotes the loss of endogenously SUMOylated proteins. We found that NME1 is a poly-SUMO1-binding protein and ML792 treatment not only decreased its polysumoylation (Fig. 3b) but also reduced the polyubiquitination of NME1 (Fig. 3c). Additionally, we transiently co-expressed FLAG-tagged NME1 and HIS-tagged SUMO1 in the HEK293T cells. Co-IP assay showed that SUMO1 overexpression boosted the polyubiquitination of NME1 (Fig. 3d), implying that SUMOylation promotes ubiquitin-mediated NME1 degradation. However, whether NME1 SUMOylation functions as a secondary signal mediating ubiquitin-dependent degradation or not remains to be verified.

We further measured HSP90α protein stability by CHX chase assays in the presence of SUMOylation or ubiquitination inhibitor. Similarly, HSP90α degradation was blocked by ML792 or MG132 treatment (Fig. 3e), indicating that intracellular HSP90α degradation is also regulated by SUMOylation or ubiquitination. Thus, we speculated that NME1 stability regulated by SUMOylation is mediated by HSP90α. To address this speculation, we examined the protein stability of NME1 in the absence of HSP90α by CHX chase assays. In HSP90AA1-deficient HEK293T cells, ML792 treatment failed to rescue NME1 degradation, while MG132 did (Fig. 3f), suggesting that increased NME1 stability following ML792 treatment is dependent on the presence of HSP90α. We further examined the effect of HSP90AA1 overexpression on the ubiquitination of NME1 by co-IP assay. Both HSP90AA1 overexpression and MG132 treatment led to increased NME1 abundance. Compared to control, HSP90AA1 overexpression diminished the polyubiquitination of NME1 regardless of whether MG132 was present or not (Fig. 3f). Together, these results suggest that SUMOylation regulates HSP90α stability which consequently modulates the lifespan of NME1.

HSP90AA1 overexpression inhibits the metastatic potential of breast cancer

Next, we investigated the effect of HSP90AA1 overexpression on the metastatic potential of breast cancer cells. First, the motilities of various types of breast cancer cells, including MCF10CA1a, 4T1 and MDA-MB-231, with altered HSP90AA1 expression were examined using the wound healing assays (Figs. 4a, b and S3B). Compared with control, stable overexpression of HSP90AA1 resulted in a significant reduction in the migration speed of human MCF10CA1a and murine 4T1 cells (Figs. 4a, b). Second, the transwell invasion assays showed that HSP90AA1 overexpression weakened the invasive ability of cells (Figs. 4c, d and S3C). Third, an in vivo orthotopic xenograft model of metastasis was used to investigate the metastatic potential of MCF10CA1a cells with HSP90AA1 or NME1 overexpression. Identical amounts of control and engineered cells were engrafted into the mammary fat pads of female BALB/c nude mice. After 8 weeks, mice were sacrificed and the volume and weight of the primary tumour were recorded. At the same time, the occurrences of metastasis to the lung were determined by H&E staining. Compared with the control, NME1 overexpression in MCF10CA1a cells did not affect growth of the primary tumour, but inhibited metastasis in the lung (Figs. 4e, f and S3D). Notably, HSP90AA1 overexpression exhibited a similar anti-metastatic activity as NME1 overexpression (Figs. 4f and S3D), but HSP90AA1 overexpression caused an increasing in the volume and weight of primary tumours (Fig. 4e).

To confirm whether the anti-metastasis activity of HSP90α is mainly mediated by the increased stability of NME1, we further assess the motility and invasiveness of the HSP90AA1-overexpressing MCF10CA1a cells whose endogenous NME1 was deficient. We silenced NME1 expression in both control and HSP90AA1-overexpressing cells using siRNA. Immunoblotting showed that the knockdown effect successfully lasted for 3 days (Fig. 4g). The wound healing assay showed that the reduced migration speed resulting from HSP90AA1 overexpression was reversed by NME1 knockdown (Fig. 4h). A similar result was also obtained in cell invasion assays (Fig. 4i). We further analysed HSP90AA1 overexpression-induced changes in the potential pathways which contribute to metastasis. Increasing experimental and clinical evidence shows that cancer cells undergo epithelial-mesenchymal transition (EMT) activated by EMT-inducing transcription factors (EMT-TFs) thus promoting motility and invasiveness and leading to enhanced metastasis. Using immunoblotting, we examined expression differences between cells overexpressing NME1 and HSP90AA1 in a series of classic EMT markers, including E-cadherin, Claudin-1, EpCAM, N-cadherin, Vimentin, β-catenin and Sox2, and in well-known EMT-TFs, including Zeb1, Snail1 and Twist1. We found that HSP90AA1 overexpression did not display the same effects on those factors as NME1 overexpression (Figs. 4j and S4A). Cells overexpressing NME1 exhibited more characteristics of epithelial cells, such as augmentation of E-cadherin and reduction of Vimentin, Zeb1 and Twist1. HSP90AA1 overexpression barely affected the expression of Claudin-1 and E-cadherin which are the important markers of epithelial cells (Figs. 4j and S4A). Among signalling pathways in the suppression of tumour

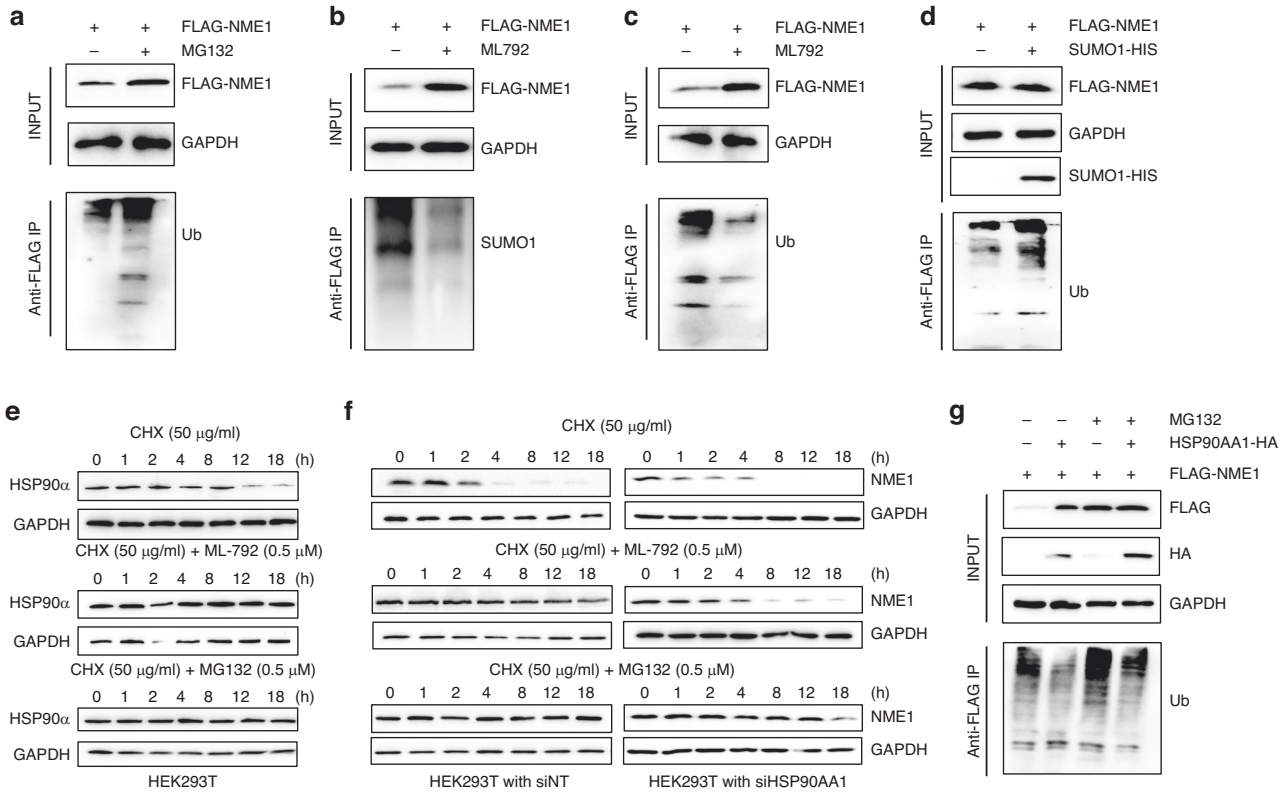

Fig. 3 SUMOylation regulates NME1 lifetime through HSP90α. a Proteasome inhibitor MG132 promoted accumulation of polyubiquitination of NME1 detected by anti-FLAG IP followed by immunoblotting with anti-ubiquitin antibody. Cell lysate for IP was prepared from HEK293T cells which exogenously expressed FLAG-tagged NME1. **b** SUMOylation inhibitor ML792 attenuated SUMO1 modification of NME1 detected by anti-FLAG IP followed by immunoblotting with anti-SUMO1 antibody. **c** SUMOylation inhibitor ML792 decreased polyubiquitination of NME1 detected by anti-FLAG IP followed by immunoblotting with anti-ubiquitin antibody. **d** SUMO1 overexpression promoted polyubiquitination of NME1 detected by anti-FLAG IP followed by immunoblotting with anti-ubiquitin antibody. Cell lysate for IP was prepared from HEK293T cells which exogenously co-expressed FLAG-tagged NME1 and HIS-tagged SUMO1. **e** HSP90α degradation upon the indicated treatment detected by CHX chase assay. **f** NME1 degradation in the control (siNT) and HSP90AA1 KD cells upon the indicated treatment detected by CHX chase assay. **g** NME1 ubiquitination was reduced by HSP90AA1 overexpression detected by anti-FLAG IP followed by immunoblotting with an anti-ubiquitin antibody. Cell lysate for IP was prepared from HEK293T cells which exogenously co-expressed FLAG-tagged NME1 and HA-tagged HSP90AA1.

metastasis, NME1 activates KSR by phosphorylation, which suppresses the activation of Raf/MEK/ERK signalling pathway, resulting in the inhibition of cell proliferation [20]. In addition, activation of AKT and p38/ERK is also modulated by NME1 which plays important roles in cell proliferation and motility [5, 21, 22]. We examined the effects of overexpression of NME1 or HSP90AA1 on these signalling pathways and found that NME1 overexpression significantly inhibits the activation of ERK, p38 and AKT by reducing their phosphorylation levels (Figs. 4k and S4B). In contrast, other than P38, HSP90AA1 overexpression robustly promoted activation of ERK and AKT, consistent with the fact that HSP90AA1 overexpression enhanced the growth of the primary tumour (Fig. 4e). Collectively, our data demonstrate that HSP90AA1 overexpression inhibits the metastatic potential of breast cancer by prolonging the lifetime of NME1. However, different from NME1 overexpression, HSP90AA1 overexpression boosts signal cascades of ERK and AKT.

Peptide OPT22 functionally imitates HSP90α to promote the stability of NME1

Since HSP90α is a molecular chaperone responsible for the maintenance of oncogenic protein homoeostasis, overexpression of HSP90AA1 is not a feasible means with which to restore the anti-metastatic function of NME1. Molecular docking using HDOCK SERVER (http://hdock.phys.hust.edu.cn/) indicates that HSP90α interacts specifically with the NME1 hexamer (Fig. 5a). To identify the domain(s) required for HSP90α function in the maintenance of NME1 stability, we cloned and stably expressed the full length and various putative NME1-interacting regions of HSP90α (Fig. 5b) in MCF10CA1a cells. Encouragingly, exogenous expression of various gene segments also elevated intracellular NME1 abundance as efficiently as intact HSP90AA1 overexpression. Among them, T22 expression exhibited the superior promoting effect on NME1 protein (Fig. 5c). Using the CHX chase assay, we compared the difference in degradation kinetics of NME1 in controls or engineered cells exogenously expressing HSP90AA1 or T22 which contains only 20 amino acids, and observed that T22 expression suppressed NME1 degradation in accordance with HSP90AA1 overexpression (Fig. 5d). Immunoblotting showed that distinct from HSP90AA1 overexpression, T22 overexpression had a similar effect as NME1 overexpression on the expression of EMT markers and EMT-TFs (Figs. 5e and S5A). Moreover, T22 overexpression also suppressed the activation of AKT, p38 and ERK (Figs. 5f and S5B).

Based on the primary structure of the T22 peptide, we synthesised a novel peptide, OPT22 fused with the known penetrating peptide TAT (Table S3). Live-cell imaging showed that FITC-labelled OPT22 (FITC-OPT22) is cell-membrane permeable (Fig. 6a). Next, we performed IP with anti-HSP90α antibody to confirm the interaction between NME1 and OPT22. HEK293T cells treated with OPT22 peptide for 4 h were subjected to immunoprecipitation and results showed that OPT22 competed with

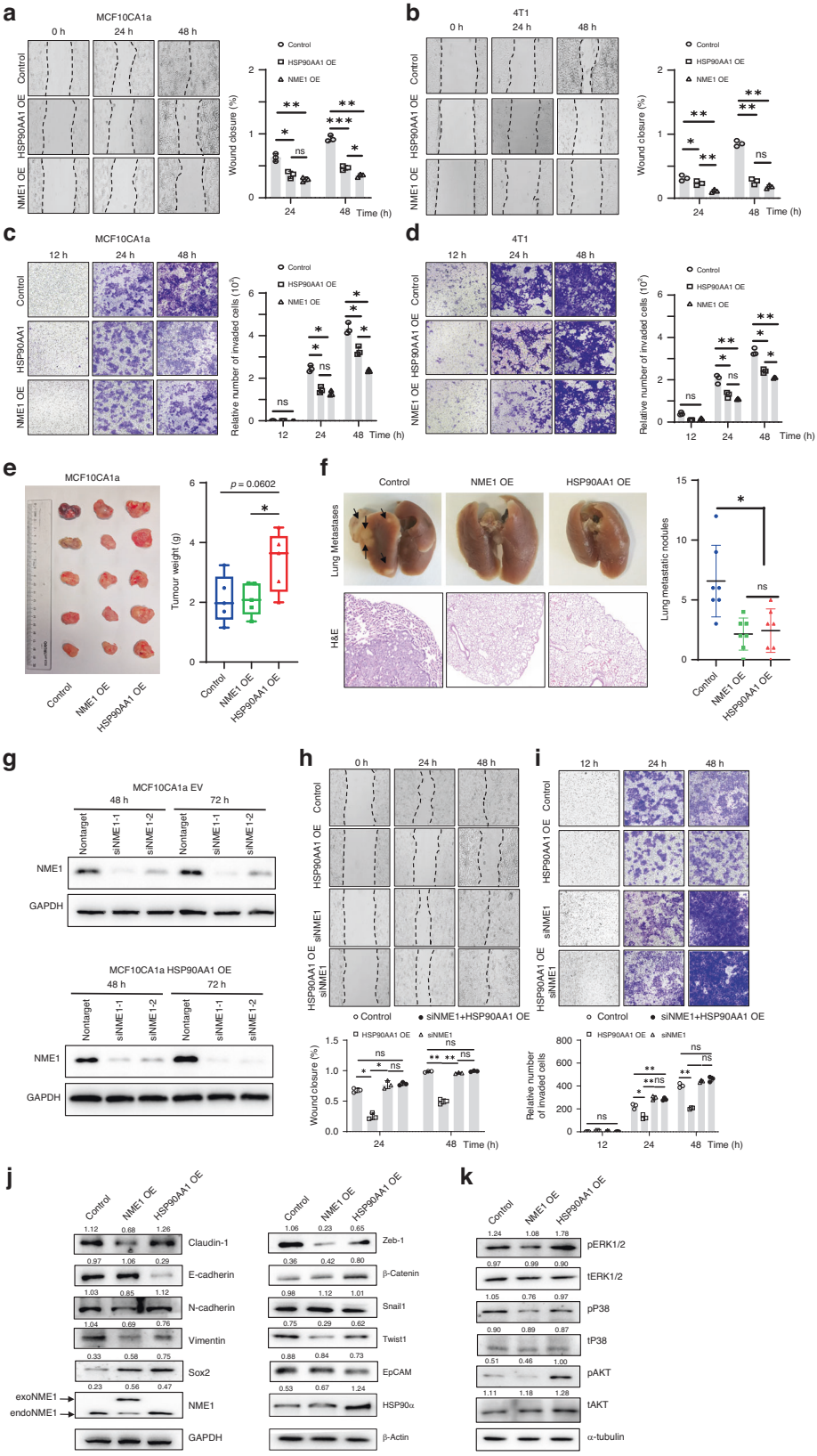

HSP90α to bind to NME1 (Fig. 6b). The CHX chase assay further confirmed that NME1 degradation in MCF10CA1a and MDA-MD-231 cells was inhibited in the presence of OPT22 (Fig. 6c). It is worth mentioning that due to its in vivo instability, OPT22 was added to medium every 4 h to maintain the effective concentration. After 12 h, MCF10CA1a cells were harvested to examine the expression of several EMT markers and EMT-TFs by immunoblotting. As expected, OPT22 treatment displayed the same effect on

Fig. 4 HSP90AA1 overexpression inhibits the metastatic potential of breast cancer cells. a, **b** Representative phase-contrast microscope images showing that HSP90AA1 overexpression attenuated motilities of MCF10CA1a (**a**) and 4T1 cells (**b**). The wound closure rates were calculated at 0, 24 and 48 h after wounding. Data are shown as the mean ± SD from three independent replicates. Student's *t*-test. $*p < 0.05$, $**p < 0.01$, $***p < 0.001$, ns, non-significant. **c**, **d** Representative images of transwell invasion assay in MCF10CA1a (**c**) and 4T1 (**d**) cells overexpressing HSP90AA1. Comparisons of the migration cell counts in different groups. Data are shown as the mean ± SD from three independent replicates. Student's *t*-test. $*p < 0.05$, $**p < 0.01$, $***p < 0.001$, ns, non-significant. **e** Photo of the excised primary tumours from female BALB/c nude mice ($n = 5$) who were orthotopically xenografted with the indicated breast cancer cells after 8 weeks (left panel). Control, NME1 OE and HSP90AA1 OE represent the engineered MCF10CA1a cells stably expressing empty vector, NME1 and HSP90AA1 gene, respectively. Tumour weight was measured and quantified (right panel). Data are shown as the mean ± SD. Student's *t*-test. $*p < 0.05$. **f** Gross anatomy of lung metastases in female BALB/c nude mice who were orthotopically xenografted with the indicated breast cancer cells after 8 weeks (upper left panel). Representative images of lung sections stained with H&E showing metastatic foci invading the pulmonary tissue (bottom left panel). Metastatic nodules were analysed and quantified microscopically (right panel). Data are shown as the mean ± SEM. One-way ANOVA test. $*p < 0.05$; ns, non-significant. **g** Immunoblotting showing that NME1 was efficiently silenced by siRNA at 48 h and 72 h in MCF10CA1a (upper panel) and HSP90AA1-overexpressing MCF10CA1a cells (bottom panel). **h** HSP90AA1 regulates cell motility mediated by NME1. The cell motility of the indicated cells was examined by the wound closure assay. Just as NME1 KD in MCF10CA1a cells, NME1 KD in HSP90AA1-overexpressing MCF10CA1a cells rescued HSP90AA1 overexpression-induced reduction in cell motility. Representative phase-contrast microscope images (upper panel) and the wound closure rate (bottom panel) are shown. Data are shown as the mean ± SD from three independent replicates. Student's *t*-test. $*p < 0.05$, $**p < 0.01$, ns, non-significant. **i** HSP90AA1 regulates cell invasiveness mediated by NME1. The cell invasiveness of the indicated cells was examined by transwell invasion assay. Just as NME1 KD in MCF10CA1a cells, NME1 KD in HSP90AA1-overexpressing MCF10CA1a cells rescued HSP90AA1 overexpression-induced reduction in cell invasiveness. The representative images of transwell invasion assays in various MCF10CA1a cells (upper panel) and comparisons of the migration cell counts in different groups (bottom panel) are shown. Data are shown as the mean ± SD from three independent replicates. Student's *t*-test. $*p < 0.05$, $**p < 0.01$, ns, non-significant. **j** Effects of NME1 or HSP90AA1 overexpression on the indicated EMT markers and EMT-TFs detected by immunoblotting. The representative images shown here are one of three biological replicates (Fig. S4A). The numbers above the gel lanes represent the relative protein levels, which were determined from the band intensity using ImageJ software, and normalised relative to the GAPDH or β-Actin loading control. endoNME1: endogenous NME1; exoNME1: exogenous NME1. **k** Effects of NME1 or HSP90AA1 overexpression on activation of p38, ERK and AKT. The phospho-ERK1/2 (Thr202/Tyr204) and total ERK1/2, phospho-P38 (Thr180/Tyr182) and total P38, phospho-AKT (Ser473) and total AKT were detected by immunoblotting. The representative images shown here are one of three biological replicates (Fig. S4B). The numbers above the gel lanes represent the relative protein levels, which were determined from the band intensity using ImageJ software, and normalised relative to the α-tubulin loading control.

the abundance of these proteins as overexpression of T22 or NME1 (Figs. 6d and S6A). Consistent with overexpression of T22 and NME1, OPT22 treatment also inhibited the activation of AKT, p38 and ERK (Figs. 6e and S6B).

We subsequently assessed the metastatic phenotype of MCF10CA1a cells treated with peptide OPT22 treatment in vitro and in vivo, respectively. The peptide consisting of a scrambled sequence of T22 fused with the penetrating TAT was used as control. Similar to overexpression of known MSGs, OPT22 treatment with various concentrations had no effect on the growth and proliferation of HEK293T and MCF10CA1a cells determined by MTT assays (Fig. 6f). Then, the effects of OPT22 on the motility and invasiveness of metastatic cancer cells, such as MCF10CA1a, MB-MDA-231 and 4T1 cells, were examined by the wound healing assay and transwell invasion assay. Both assays showed that OPT22 treatment significantly inhibited cell motility (Figs. 6g and S7A, C) and invasiveness in vitro (Figs. 6h and S7B, D). We further examined the anti-metastasis efficacy of OPT22 in an orthotopic allograft murine model (the spontaneous metastasis model). 4T1 mouse breast cancer cells were injected into the mammary gland of host mice. OPT22 peptide was administrated by peritumor injection twice a day for 2 weeks and the metastases of 4T1 cells into the lung were examined with a colonogenic assay (schematic as shown in Fig. S8A upper panel). We found that there was no significant difference of primary tumour volume and weight between control and OPT22 treatment group (Fig. 6i). However, H&E-stained primary tumour sections revealed that OPT22 significantly increased protein level of NME1 (Fig. 6k). Encouragingly, compared with control group, OPT22-treated mice had a lower number of tumour colonies developed in the lung (Fig. 6j and S8A bottom panel). We also evaluate the anti-metastasis function of OPT22 in the tail vein injection model of metastasis. MCF10CA1a human breast cancer cells were injected into the tail vein of nude immunodeficient mice. After 1 week, OPT22 peptide was administrated by intraperitoneal injection twice a day for 4 weeks. The colonisation of MCF10CA1a cells in the lung was detected by H&E stain (schematic as shown in Fig. S8B upper panel). The number of metastases formed in the lungs was microscopically counted per 5 μm lung section per mouse that had the most metastatic lesions. As we expected, OPT22 treatment significantly reduced metastatic colonisation of MCF10CA1a cells (Fig. S8B bottom panel and details in S8C). Collectively, our data demonstrated that the new peptide, OPT22 mimics the function of HSP90AA1 and strongly inhibits the metastatic potential of cancer cells.

DISCUSSION

Currently, metastasis remains the main challenge in treating cancer. Encouragingly, the discovery of MSGs has provided potential therapeutic targets for metastatic disease and attracted increasing interest in translational research. NME1, the first identified metastasis suppressor, has been the focus of therapeutic targets for decades. To restore the anti-metastatic function of NME1, upregulation of its intracellular expression is considered to be effective. However, current strategies including transcriptional transactivation, gene therapy and delivery of recombinant protein, overlook the fact that intracellular abundance of NME1 is strictly regulated by degradation pathways. In this study, we discovered the new regulatory mechanism underlying NME1 degradation in breast cancer cells. Based on our findings, we designed and synthesised a cell-permeable therapeutic peptide, OPT22 which successfully mimics HSP90α function and prolongs the life span of NME1. The anti-metastasis function of OPT22 which was confirmed in vivo in the different murine models of metastasis suggests its potential use in metastatic cancer therapy.

Accumulating evidence demonstrates that the oligomeric structure of NME1 is not only intimately associated with its phosphotransferase activity either towards NDP phosphorylation or protein-histidine phosphorylation, but also affects its intracellular protein abundance [23–27]. NME1 usually forms a hexamer with a D3 symmetry which consists of a trimer of dimers. Crystal structure analysis has shown that the N-terminal region (20–41 residues) forms the bulk of the dimeric interface [28]. Li et al. also found that point mutations of clusters 21–23 or 38–40 attenuate the expression level of NME1 [29]. The C-terminal region (134–151

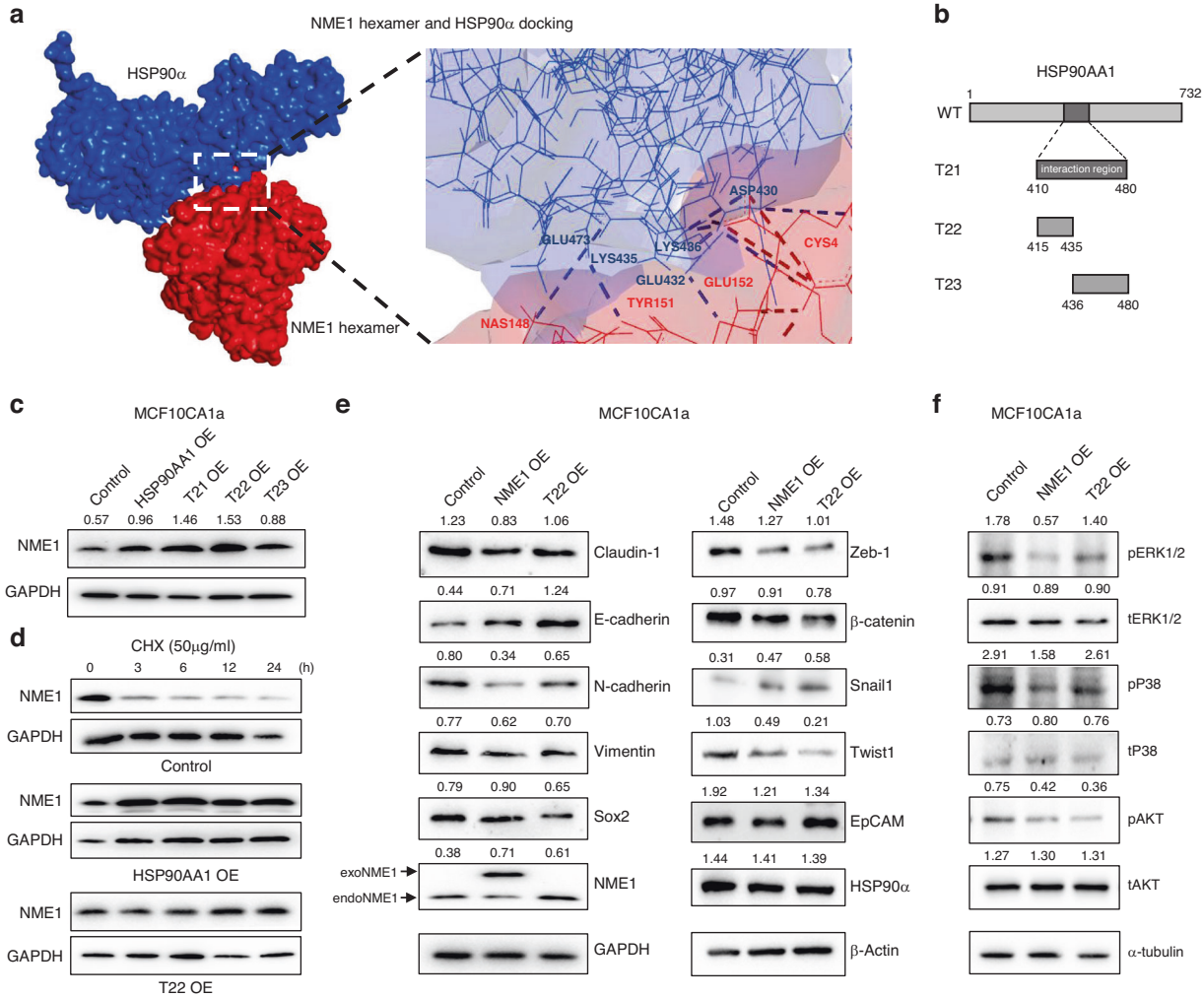

Fig. 5 Expression of NME1-binding domain of HSP90α improves the lifetime of NME1. a Protein docking simulating specific interaction of HSP90α with NME1 hexamer. At the putative HSP90α-NME1 hexamer interface, residues (Asp 430, Glu432, Lys435, Lys436 and Glu473 of HSP90α and Cys4, Asn148, Tyr151 and Glu152 of NME1) are involved in interaction. **b** Schematic of the putative NME1-interacting domain of HSP90α (T21) and truncates (T22 and T23). **c** Effects of overexpression of T21, T22 and T23 on intracellular NME1 abundance detected by immunoblotting. **d** Overexpression of T22 inhibited NME1 degradation detected by CHX chase assay. **e** Effects of NME1 or T22 overexpression on the indicated EMT markers and EMT-TFs detected by immunoblotting. The representative images shown here are one of three biological replicates (Fig. S5A). The numbers above the gel lanes represent the relative protein levels, which were determined from the band intensity using ImageJ software, and normalised relative to the GAPDH or β-Actin loading control. **f** Effects of NME1 or T22 overexpression on activation of p38, ERK and AKT detected by immunoblotting. The representative images shown here are one of three biological replicates (Fig. S5B). The numbers above the gel lanes represent the relative protein levels, which were determined from the band intensity using ImageJ software, and normalised relative to the α-tubulin loading control.

residues) participates in interactions within the dimer and between monomers in the trimers [28]. In our study, we observed that deletions at the N-terminus (T1 ($\Delta^{1\text{-}20}$) and T7 ($\Delta^{21\text{-}55}$)) abolished oligomerization of NME1, while T5 with C-terminal deletion ($\Delta^{133\text{-}152}$) still formed dimer, but very few trimer or tetramer (Fig. 1f), implying that the regions at the N-terminus are more important for protein folding and oligomerization, compared with the C-terminal region. Additionally, NME1-NME2 can form homo- and hetero-hexamers. We found that HSP90α also increased the intracellular abundance of NME2 but not as efficiently as NME1 (Fig. 2h). Available data suggest a strong correlation between oligomerization and protein stability, but the mechanism underlying this correlation remains elusive. Herein, we have defined for the first time the important role of HSP90α in maintaining homoeostasis of NME1. The fact that HSP90α especially interacts with NME1 hexamer predicted by protein-protein docking explains very well the relationship between oligomerization and protein stability.

HSP90 is highly conserved and ubiquitously expressed in eukaryotic cells. As a molecular chaperone, HSP90 is required for the maturation and activation of numerous substrate proteins (referred to as client proteins) many of which play important roles in cell cycle control, cellular stress response, and signal transduction [30]. In the list of known HSP90 interactors summarised by Dr. Didier Picard, many client proteins are either kinases or transcription factors which take part in multiple oncogenic signaling pathways [31]. Thus, interactions between HSP90 and client proteins are essential processes in tumour survival, proliferation and migration [32]. Cytoplasmic HSP90α and HSP90β are major HSP90 isoforms in humans intensively and extensively studied [18, 33]. Our xenograft model also validated the pro-tumour activity of HSP90α in the primary tumour (Fig. 4e). At the same time, we demonstrated that HSP90α also suppresses the metastatic potential of breast cancer by protecting endogenous NME1 against degradation. Therefore, HSP90 functions as a key driver of the "Grow" or "Go" model for cancer migration and progression

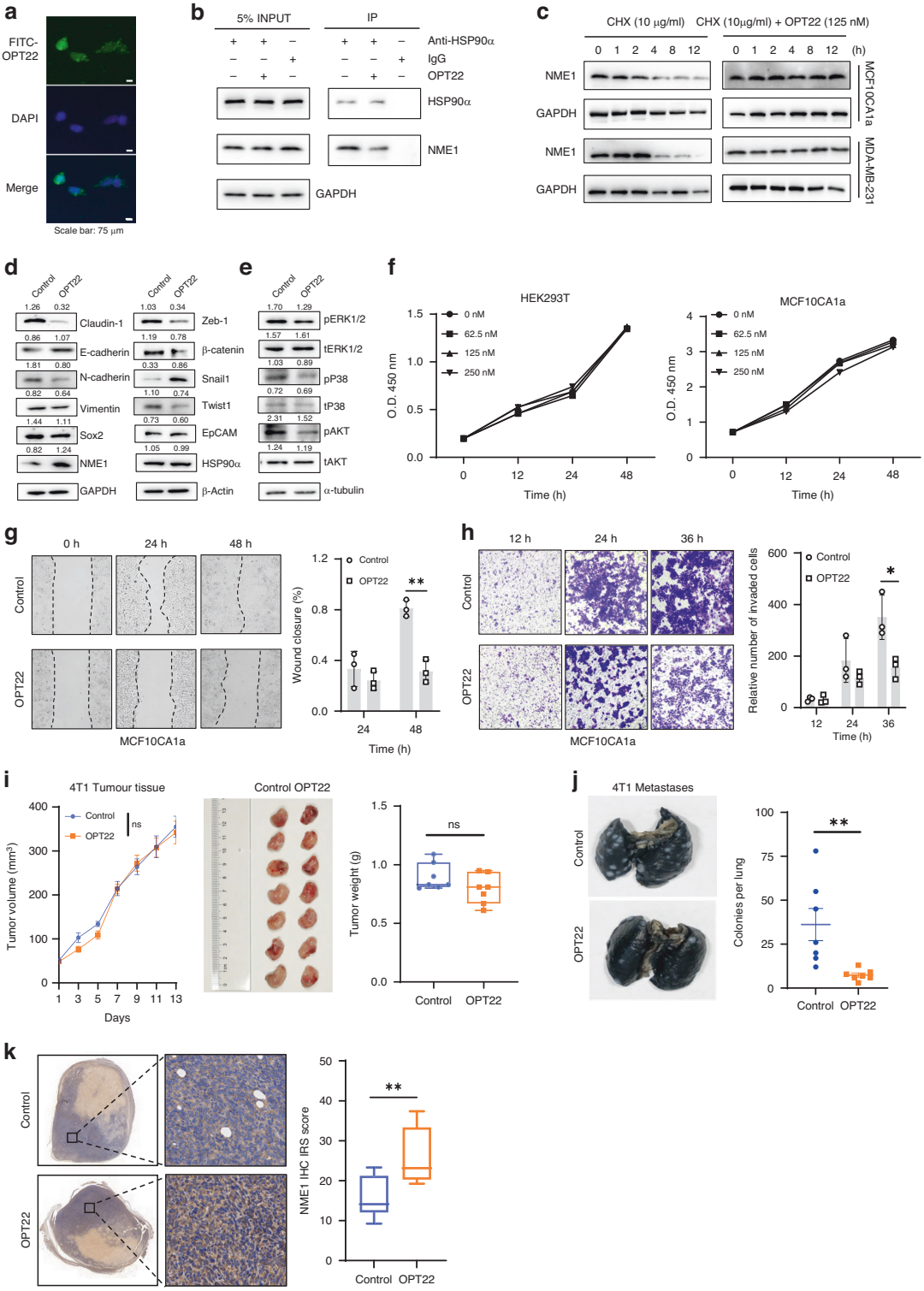

[34, 35]. Additionally, it is noteworthy that the role of EMT in vivo in metastasis is now becoming debatable. Current studies using an EMT lineage-tracking system or mouse models of pancreatic ductal adenocarcinoma (PDAC) with Sail or Twist deletion question the contribution of EMT to metastasis [36, 37]. Although exhibiting distinct effects on some EMT markers and transcription factors, HSP90AA1 overexpression suppressed the metastatic potential of breast cancer as efficiently as NME1 overexpression both in vitro and in vivo assays. We found that some important factors involved in metastasis including Vimentin, β-catenin, Twist1, p38, and AKT, are also interactors of HSP90. These findings, on the one side, well explained the reason why HSP90AA1 overexpression has more complicated effects on levels of these proteins compared to NME1 overexpression; on the other side, challenged the known functional roles of these proteins in metastasis. We believe that comprehensive elucidation of HSP90 function in metastasis will foster our understanding of the EMT process and its contribution to metastasis.

Fig. 6 Peptide OPT22 functionally imitates HSP90α to promote NME1 stability. a Live-cell image showing the membrane penetration ability of the FITC-labelled peptide OPT22. MCF10CA1a cells were treated by FITC-OPT22 peptide (125 nM) for 30 min. **b** Co-IP assay using anti-HSP90α showing that the presence of OPT22 peptide (125 nM) attenuated interaction between HSP90α and NME1. MCF10CA1a cells were treated with OPT22 for 4 h prior to cell lysis. **c** Effect of OPT22 treatment (125 nM) on NME1 degradation in MCF10CA1a and MDA-MB-231 cells detected by CHX chase assay. **d** Expression of the indicated EMT markers and EMT-TFs upon OPT22 treatment (125 nM) detected by immunoblotting. The experiment was independently repeated at least three times (Fig. S6A). The representative images are shown here. The numbers above the gel lanes represent the relative protein levels, which were determined from the band intensity using ImageJ software, and normalised relative to the GAPDH or β-Actin loading control. **e** Activation of ERK, p38 and AKT upon OPT22 treatment detected by immunoblotting. The experiment was independently repeated at least three times (Fig. S6B). The representative images are shown here. The numbers above the gel lanes represent the relative protein levels, which were determined from the band intensity using ImageJ software, and normalised relative to the α-tubulin loading control. **f** Effects of OPT22 treatment with various concentrations on the proliferation of HEK293T cells and MCF10CA1a cells detected by the CCK8 assay. Data are the mean ± SD of three independent replicates. Student's *t*-test. **g** Representative images (left panel) and the wound closure rate (right panel) showing that cell motility was attenuated upon OPT22 treatment (125 nM) examined by the wound healing assay. Data are shown as the mean ± SD from three independent replicates. Student's *t*-test. $^{*}p < 0.05$, $^{**}p < 0.01$. **h** Representative images of transwell invasion assay in MCF10CA1a cells treated with OPT22 (125 nM) (left panel). Comparisons of the migration cell count in different groups (right panel). Data are shown as the mean ± SD from three independent replicates. Student's *t*-test. $^{*}p < 0.05$, $^{**}p < 0.01$. **i** Effect of OPT22 peptide treatment on the growth of primary tumour. 4T1 cell allograft metastasis mouse model was set up and OPT22 and control peptides were administrated by peritumor injection (50 μg/mouse) twice a day for 2 weeks. Tumour volume was monitored every other day for 13 days (left panel). Photo of the excised tumours from mice ($n = 7$) with different treatments (middle panel) and tumour weight (right panel) are shown. Student's *t*-test. ns, non-significant. **j** Evaluation of therapeutic effect of OPT22 peptide on metastasis using 4T1 cell allograft metastasis mouse model. Representative images showing macroscopic surface metastases in lungs stained with India ink in mice with different treatments (left panel). An average number of colonies in the lungs ($n = 7$) is calculated (right panel). Data are shown as the mean ± SEM. Student's *t*-test. $^{**}p < 0.001$. **k** IHC representative images of primary tumour tissues using NME1 antibody (left panel). Scale bars for ×10 images: 500 μm; scale bars for ×200 images: 20 μm. Statistical analysis of NME1 IHC IRS score of primary tumour tissues (right panel). Student's *t*-test. Data are shown as the mean ± SD. $^{**}p < 0.01$.

HSP90 is considered a potential target for cancer therapy [33]. Inhibition of HSP90 leads to client proteins to undergo ubiquitination-proteasome degradation. A variety of HSP90 inhibitors have been developed and shown promising antitumor effects. Therefore, upregulation of HSP90α is not a suitable approach for metastatic cancer therapy. In this study, a novel cell-permeable peptide OPT22 was adopted to mimic the function of HSP90α and successfully prolonged the life span of endogenous NME1, resulting in declined cell motility and invasiveness. OPT22 treatment also exhibited superior anti-metastatic efficacy in the different mouse models of metastasis. Immunoblotting showed that OPT22 treatment had nearly the same effects on the expression of indicated EMT markers and kinases as NME1 overexpression, eliminating the side effect of HSP90AA1 overexpression. However, OPT22 as a drug candidate still has significant shortcomings, such as poor oral bioavailability, plasma stability, membrane permeability and circulation half-life [38]. Optimisation of the properties of the OPT22 is an imperative demand for its clinic use. Nonetheless, the anti-metastatic activity of OPT22 not only verifies our findings that HSP90α regulates NME1 stability, but also paves the way for developing a new approach or drug for metastatic cancer therapy.

MATERIAL AND METHODS

Tissue specimens, cell culture and reagents

The primary tumour tissues and metastases in lymph nodes from breast cancer patients were obtained from the Nanjing People's Hospital (Jiangsu, China) and approved for study by the Institutional Review Board of Nanjing People's Hospital.

The breast cancer cell lines, including MCF-7, MCF10CA1a, MDA-MB-231, 4T1 and HEK293T cells were provided as gifts by Judy Lieberman's lab at Boston Children's Hospital, Harvard Medical School. MDA-MB-468, BT474 and T47D cells were purchased from the Cell Bank, Shanghai Institutes for Biological Sciences, CAS. Cells were maintained in DMEM (KevGen, China) supplemented with 10% fetal bovine serum (FBS) (Homeland, China), 100 U/ml penicillin, and 100 μg/ml streptomycin at 37 °C in a humidified incubator (5% CO_2). All cell lines were verified to be free of mycoplasma contamination.

MG132 (GC10383) was purchased from GlpBio. 3-Methyladenine (3-MA) (5142-23-4) was from Sigma-Aldrich. Chloroquine (S6999) and ML-792 (HY-108702) were from Selleck. Glutaraldehyde (A600875) was obtained from Sangon Biotech. The control and OPT22 peptides were synthesised by Genscript Biotech.

Mouse models of metastasis

Different metastasis mouse models were established to assess the metastatic potential of the indicated breast cancer cells. For the orthotopic allograft or xenograft model, briefly, 5×10^5 breast cancer cells as indicated mixed with matrigel were transplanted into the mammary fat pad of female BALB/c wide type ($n = 7$) or nude mice ($n = 8$). For the xenograft metastasis model by tail vein injection, the anaesthetised BALB/c nude mice ($n = 8$) were injected intravenously (caudal vein) with 5×10^5 breast cancer cells as indicated. The volume of primary tumour and mouse weight were monitored weekly. After 5–8 weeks, mice were sacrificed. To examine lung metastases, lung tissue was harvested and fixed in 4% paraformaldehyde overnight. Sections 20 μm in thickness were mounted on slides. H&E staining was performed on the lung sections and metastatic nodules were analysed microscopically.

All animal procedures and experiments in this study were approved by the Ethics of Animal Experiments of Xinjiang Key Laboratory of Biological Resources and Genetic Engineering (BRGE-AE001) and the Ethics Committee of China Pharmaceutical University (Permit Number: SYXK2012-0035).

RNA interference and qPCR

The expression of both HSP90AA1 and HSP90AB1 in breast cancer cells was knocked down by siRNA. The siRNA duplexes targeting HSP90AA1 and HSP90AB1 were chemically synthesised by General Biology. The siRNA sequences are listed in Table S1 in the Supplementary Information (SI). siRNA was transfected with Lipofectamine 2000 (Invitrogen) according to the manufacturer's instructions. The efficiency of knockdown was examined by RT-qPCR. The total RNA was extracted from cells using TRIzol® Reagent (Life Technologies). First-strand cDNA for qPCR was synthesised using Hifair® III1st Strand cDNA Synthesis SuperMix (Yeasen). Real-time qPCR was performed using AceQ SYBR Green Master Mix (Vazyme). Reactions were carried out in the 7300Plus Real-Time PCR System (Thermo Fisher) with gene-specific primers. The sequences of primers used in this study are listed in SI, Table S1.

Immunoblotting, immunofluorescence and immunohistochemistry

For immunoblotting, protein samples were prepared from cultured cells using a RIPA lysis buffer containing a protease and phosphatase inhibitor cocktail (NCM biotech). After separation by sodium dodecyl-sulfate polyacrylamide gel electrophoresis (SDS-PAGE), proteins were transferred to the sheet of a poly(vinylidene fluoride) membrane (Millipore). The target protein was detected by incubating membranes with a specific primary antibody overnight at 4 °C, followed by HRP-conjugated secondary antibody incubation. Subsequently, the protein–antibody complex was

visualised by enhanced chemiluminescence assay (Tanon). Each immunoblotting experiment was conducted at least twice independently. The representative images are shown in the Figures. For quantitative analysis, the numbers above the gel lanes represent the relative protein levels, which were determined from the band intensity using ImageJ software, and normalised relative to the GAPDH, β-Actin or α-tubulin loading control.

For immunofluorescence, cells were cultured on glass slides. Upon reaching 50% confluency, cells were fixed with 4% formaldehyde, followed by permeabilization with PBS buffer containing 0.2% Triton X-100. After being blocked with 10% goat serum, cells were sequentially incubated with the indicated primary antibody overnight with 1:150 dilution, followed by incubation with the appropriate fluorescence-conjugated secondary antibody with 1:500 dilution. DAPI was used to stain nuclei and confocal images were obtained using a Zeiss LSM 800 confocal microscopy system.

For immunohistochemical (IHC) analysis, formalin-fixed paraffin-embedded tissue blocks were obtained from the pathology archive of Jiangsu People's Hospital. Tumour tissue slides were deparaffinized, rehydrated with a series of alcohol treatments, and then subjected to antigen retrieval with sodium citrate buffer. Block tumour sections were treated with 5% normal goat serum, 0.1% Triton X-100, and 3% H_2O_2 in PBS for 60 min at room temperature, respectively, then incubated with appropriate antibodies (1:200 dilution) overnight at 4 °C. IHC staining using DAB detection conjugated with horseradish peroxidase (HRP). The IHC slides were scored to assess the staining intensity ordinal value.

Antibodies used in this study are listed in Table S2 in the SI.

Recombinant protein purification and oligomeric analysis

The genes encoding NME1 wild type and truncates were cloned into a pET28a vector and expressed in *E. coli*. The recombinant proteins with HIS-Tag were purified using nickel resin affinity chromatography according to the manufacturer's instructions. After being checked by SDS-PAGE gel stained with Coomassie blue, the eluted proteins were thoroughly dialysed in buffer D (20 mM Tris–HCl pH 7.9, 20% glycerol, 100 mM KCl, 0.2 mM EDTA and 1 mM DTT) at 4 °C. For oligomeric analysis, 20 μmole recombinant protein was pre-incubated in PBS containing 5 mM DTT for 30 min at room temperature. Then, 2 mM glutaraldehyde was added to initiate the cross-linking. After 30 min incubation, the reaction was quenched with 0.2 M Tris–HCl, pH 7.4, for 15 min. The reaction product was subjected to protein electrophoresis analysis using 4–12% Bis-Tris SDS-PAGE gel and visualised by protein staining with Coomassie brilliant blue.

Immunoprecipitation (IP)

Cells were lysed in IP buffer (25 mM Tris–HCl, 150 mM NaCl, 1% NP-40 and 5% glycerol at pH 7.4), supplemented with protease and phosphatase inhibitors. After centrifugation, the supernatant was collected for immunoprecipitation. Relevant antibodies (3 μg) were added to the cell lysates and incubated overnight at 4 °C with gentle rotation. Then, 10 μl of protein A/G dynabeads were added to the cell lysate-antibody mixture and incubated at 4 °C for 3 h with rotation. Pellet dynabeads were isolated using a magnetic separation rack and the supernatant was discarded. After extensive washing, the pellet was resuspended in 30 μl SDS elution buffer and boiled for 5 min. The supernatant was subjected to immunoblotting analysis. For the analysis of NME1 interactome, IP products immunoprecipitated by anti-FLAG antibody were resuspended in PBS, followed by mass spectrometric analysis by the Novogene company.

Wound healing and transwell invasion assays

Approximately 6×10^5 cells were seeded into a 6-well culture plate. On the following day, confluent monolayers of cells were scratched with a sterile micropipette tip. Cells were gently washed twice with PBS to remove detached or dead cells. The well was replenished and treated with fresh serum-free medium, followed by incubation at 37 °C for the indicated time. Phase-contrast images of the wounded area were recorded using an inverted microscope at the indicated time points. Wound area measurement was performed by digital planimetry using Image J software. The wound closure rate was calculated as the ratio of the difference between the original wound area and the healing area to the original wound area × 100%.

Matrigel (10 mg/ml) diluted at 4:1 in DMEM medium was plated on the transwell membranes and air-dried. 1×10^5 cells were seeded into the top chambers of the transwell plates in FBS-free media. Then, 0.5 ml DMEM supplemented with 5% FBS was added to the well of the plate (the lower compartment) to stimulate cell migration. The plates were incubated at 37 °C for 12, 24 and 36 h, respectively. The invasive cells that migrated to the lower surface of the membrane were fixed with 4% paraformaldehyde for 15 min and then stained with 0.1% crystal violet for 20 min at room temperature. After washing, the invasive cells were visualised and counted under an optical microscope.

OPT22 peptide treatment

Female BALB/c mice at 6 weeks of age were injected with 5×10^5 4T1 cells mixed with 50 μl Matrigel (Yeasen) subcutaneously into fat pads near the hind limbs. When implanted tumours began to appear, the mice were divided into two groups randomly and treated with control and OPT22 peptide (50 μg/mouse), respectively, by peritumor injection twice a day for 2 weeks. Mice were euthanized at 9 weeks of age. The primary tumours and lung tissues were harvested for subsequent analysis.

Female BALB/c nude mice at 6 weeks of age were injected with 5×10^5 MCF10CA1a cells by tail vein. One week after injection, the mice were divided into two groups randomly and treated with control and OPT22 peptide (50 μg/mouse), respectively, by intraperitoneal injection twice a day for 4 weeks. At the end of the experiment, the lung tissue of each mouse was harvested for metastasis analysis.

Statistical analysis

Statistical analysis was performed using Graphpad software (version 8.0). Data were presented as the mean ± SD and analysed using Student's *t*-test or one-way analysis of variance (ANOVA) test. $^*p < 0.05$; $^{**}p < 0.01$, and $^{***}p < 0.001$, $^{****}p < 0.0001$. A *p*-value less than 0.05 was considered statistically significant.

DATA AVAILABILITY

All data generated or analysed in this study that are relevant to the results presented in this article are included in this article and its supplementary information files (Additional files). Other data that were not relevant to the results presented here are available from the corresponding author upon reasonable request.

REFERENCES

1. Yoshida BA, Sokoloff MM, Welch DR, Rinker-Schaeffer CW. Metastasis-suppressor genes: a review and perspective on an emerging field. J Natl Cancer Inst. 2000;92:1717–30.
2. Steeg PS, Bevilacqua G, Kopper L, Thorgeirsson UP, Talmadge JE, Liotta LA, et al. Evidence for a novel gene associated with low tumor metastatic potential. J Natl Cancer Inst. 1988;80:200–4.
3. Yu L, Wang X, Zhang W, Khan E, Lin C, Guo C. The multiple regulation of metastasis suppressor NM23-H1 in cancer. Life Sci. 2021;268:118995.
4. Kuo KT, Chen CL, Chou TY, Yeh CT, Lee WH, Wang LS. Nm23H1 mediates tumor invasion in esophageal squamous cell carcinoma by regulation of CLDN1 through the AKT signaling. Oncogenesis 2016;5:e239.
5. Li MQ, Shao J, Meng YH, Mei J, Wang Y, Li H, et al. NME1 suppression promotes growth, adhesion and implantation of endometrial stromal cells via Akt and MAPK/Erk1/2 signal pathways in the endometriotic milieu. Hum Reprod. 2013;28:2822–31.
6. Marshall JC, Collins J, Marino N, Steeg P. The Nm23-H1 metastasis suppressor as a translational target. Eur J Cancer. 2010;46:1278–82.
7. Ouatas T, Halverson D, Steeg PS. Dexamethasone and medroxyprogesterone acetate elevate Nm23-H1 metastasis suppressor gene expression in metastatic human breast carcinoma cells: new uses for old compounds. Clin Cancer Res. 2003;9:3763–72.
8. Lim J, Jang G, Kang S, Lee G, Nga do TT, Phuong, et al. Cell-permeable NM23 blocks the maintenance and progression of established pulmonary metastasis. Cancer Res. 2011;71:7216–25.
9. Chen W, Xiong S, Li J, Li X, Liu Y, Zou C, et al. The ubiquitin E3 ligase SCF-FBXO24 recognizes deacetylated nucleoside diphosphate kinase A to enhance its degradation. Mol Cell Biol. 2015;35:1001–13.
10. Fiore LS, Ganguly SS, Sledziona J, Cibull ML, Wang C, Richards DL, et al. c-Abl and Arg induce cathepsin-mediated lysosomal degradation of the NM23-H1 metastasis suppressor in invasive cancer. Oncogene. 2014;33:4508–20.
11. Khera L, Paul C, Kaul R. Hepatitis C Virus E1 protein promotes cell migration and invasion by modulating cellular metastasis suppressor Nm23-H1. Virology. 2017;506:110–20.
12. Paul C, Khera L, Kaul R. Hepatitis C virus core protein interacts with cellular metastasis suppressor Nm23-H1 and promotes cell migration and invasion. Arch Virol. 2019;164:1271–85.

13. Holliday DL, Speirs V. Choosing the right cell line for breast cancer research. Breast Cancer Res. 2011;13:215.
14. Dai X, Cheng H, Bai Z, Li J. Breast cancer cell line classification and its relevance with breast tumor subtyping. J Cancer. 2017;8:3131–41.
15. Singh B, Tai K, Madan S, Raythatha MR, Cady AM, Braunlin M, et al. Selection of metastatic breast cancer cells based on adaptability of their metabolic state. PLoS ONE. 2012;7:e36510.
16. Hartsough MT, Clare SE, Mair M, Elkahloun AG, Sgroi D, Osborne CK, et al. Elevation of breast carcinoma Nm23-H1 metastasis suppressor gene expression and reduced motility by DNA methylation inhibition. Cancer Res. 2001;61:2320–7.
17. Yu BYK, Tossounian MA, Hristov SD, Lawrence R, Arora P, Tsuchiya Y, et al. Regulation of metastasis suppressor NME1 by a key metabolic cofactor coenzyme A. Redox Biol. 2021;44:101978.
18. Schopf FH, Biebl MM, Buchner J. The HSP90 chaperone machinery. Nat Rev Mol Cell Biol. 2017;18:345–60.
19. Ciechanover A, Schwartz AL. The ubiquitin-proteasome pathway: the complexity and myriad functions of proteins death. Proc Natl Acad Sci USA. 1998;95:2727–30.
20. Salerno M, Palmieri D, Bouadis A, Halverson D, Steeg PS. Nm23-H1 metastasis suppressor expression level influences the binding properties, stability, and function of the kinase suppressor of Ras1 (KSR1) Erk scaffold in breast carcinoma cells. Mol Cell Biol. 2005;25:1379–88.
21. Hua K, Feng W, Cao Q, Zhou X, Lu X, Feng Y. Estrogen and progestin regulate metastasis through the PI3K/AKT pathway in human ovarian cancer. Int J Oncol. 2008;33:959–67.
22. Zhang X, Fu LJ, Liu XQ, Hu ZY, Jiang Y, Gao RF, et al. nm23 regulates decidualization through the PI3K-Akt-mTOR signaling pathways in mice and humans. Hum Reprod. 2016;31:2339–51.
23. Abu-Taha IH, Vettel C, Wieland T. Targeting altered Nme heterooligomerization in disease? Oncotarget. 2018;9:1492–3.
24. Chen Y, Qian C, Guo C, Ge F, Zhang X, Gao X, et al. A Cys/Ser mutation of NDPK-A stabilizes its oligomerization state and enhances its activity. J Biochem. 2010;148:149–55.
25. Kim YI, Park S, Jeoung DI, Lee H. Point mutations affecting the oligomeric structure of Nm23-H1 abrogates its inhibitory activity on colonization and invasion of prostate cancer cells. Biochem Biophys Res. Commun. 2003;307:281–9.
26. Postel EH. NM23-NDP kinase. Int J Biochem Cell Biol. 1998;30:1291–5.
27. Souza TA, Trindade DM, Tonoli CC, Santos CR, Ward RJ, Arni RK, et al. Molecular adaptability of nucleoside diphosphate kinase b from trypanosomatid parasites: stability, oligomerization and structural determinants of nucleotide binding. Mol Biosyst. 2011;7:2189–95.
28. Webb PA, Perisic O, Mendola CE, Backer JM, Williams RL. The crystal structure of a human nucleoside diphosphate kinase, NM23-H2. J Mol Biol. 1995;251:574–87.
29. Li YJ, Liu W, Saini V, Wong YH. Mutations at the dimer interface and surface residues of Nm23-H1 metastasis suppressor affect its expression and function. Mol Cell Biochem. 2020;474:95–112.
30. Wayne N, Mishra P, Bolon DN. Hsp90 and client protein maturation. Methods Mol Biol. 2011;787:33–44.
31. Echeverria PC, Bernthaler A, Dupuis P, Mayer B, Picard D. An interaction network predicted from public data as a discovery tool: application to the Hsp90 molecular chaperone machine. PLoS ONE. 2011;6:e26044.
32. Li ZN, Luo Y. HSP90 inhibitors and cancer: prospects for use in targeted therapies (Review). Oncol Rep. 2023;49:6.
33. Hahn JS. The Hsp90 chaperone machinery: from structure to drug development. BMB Rep. 2009;42:623–30.
34. Giese A, Loo MA, Tran N, Haskett D, Coons SW, Berens ME. Dichotomy of astrocytoma migration and proliferation. Int J Cancer. 1996;67:275–82.
35. Hatzikirou H, Basanta D, Simon M, Schaller K, Deutsch A. 'Go or grow': the key to the emergence of invasion in tumour progression? Math Med Biol. 2012;29:49–65.
36. Fischer KR, Durrans A, Lee S, Sheng J, Li F, Wong ST, et al. Epithelial-to-mesenchymal transition is not required for lung metastasis but contributes to chemoresistance. Nature. 2015;527:472–6.
37. Zheng X, Carstens JL, Kim J, Scheible M, Kaye J, Sugimoto H, et al. Epithelial-to-mesenchymal transition is dispensable for metastasis but induces chemoresistance in pancreatic cancer. Nature. 2015;527:525–30.
38. Otvos L Jr, Wade JD. Current challenges in peptide-based drug discovery. Front Chem. 2014;2:62.

ACKNOWLEDGEMENTS

This work was supported by National Natural Science Foundation of China grants (32370627, 82360605, 81773028).

AUTHOR CONTRIBUTIONS

YCZ and GMZ were responsible for designing the work, acquiring data and interpreting main results. LTY, XDW, YM and JLM validated some results and performed bioinformatic analysis. ZYF and YMY collected tumour samples from cancer patients and performed IHC analysis. JYL and XW managed the programme and drug efficacy evaluation. CYG was responsible for supervision, funding acquisition and manuscript preparation.

COMPETING INTERESTS

The authors declare no competing interests.

ADDITIONAL INFORMATION

Supplementary information The online version contains supplementary material available at https://doi.org/10.1038/s41416-023-02435-3.

Correspondence and requests for materials should be addressed to Yongmei Yin, Jinyao Li, Xun Wang or Changying Guo.